International Journal of Biological Macromolecules 103 (2017) 111–119

Contents lists available at ScienceDirect

International Journal of Biological Macromolecules

journal homepage: www.elsevier.com/locate/ijbiomac

pH induced single step shift of hydrophobic patches followed by formation of an MG state and an amyloidogenic intermediate in Lima Bean Trypsin Inhibitor (LBTI)

Javed Masood Khan[a,*], Mohammad A. Alsenaidy[b], Mohd Shahnawaz Khan[c], Priyankar Sen[d], Rizwan Hasan Khan[e], Sadaf Fatima[f,*]

[a] Department of Food Science and Nutrition, Faculty of Food and Agricultural Sciences, King Saud University, 2460, Riyadh 11451, Saudi Arabia
[b] Department of Pharmaceutics, College of Pharmacy, King Saud University, Riyadh, Saudi Arabia
[c] Protein Research Chair, Department of Biochemistry, College of Science, King Saud University, Riyadh, Saudi Arabia
[d] Centre for Bioseparation Technology, VIT University, Vellore 632014, India
[e] Interdisciplinary Biotechnology Unit, Aligarh Muslim University, Aligarh, India
[f] Department of Biotechnology, Jamia Millia Islamia, New Delhi, India

ARTICLE INFO

Article history:
Received 26 January 2017
Received in revised form 1 May 2017
Accepted 9 May 2017
Available online 10 May 2017

Keywords:
Lima Bean Trypsin Inhibitor
Protein folding intermediates
Molten globule
Protein aggregation

ABSTRACT

Lima Bean Trypsin Inhibitor (LBTI) is 83 residues monomeric protein of 9.0 KDa, consisting of six antiparallel β-strands and can undergo concentration dependant dimerization. We have tried to characterize folding intermediates of LBTI under equilibrium denaturation conditions. We have used various spectroscopic and microscopic techniques to understand the folding and misfolding pathways. LBTI forms molten globule structure at pH 2 and amyloidiogenic intermediate state (I^a) at pH 4. pH induced Shifting of surface exposed hydrophobic patches and that followed by withdrawal of the lone tyrosine residue (Y69) towards nonpolar environment have been reported. Denaturation profile of native and molten globule (MG) states of LBTI in presence of guanidine hydrochloride show sigmoidal curves with non-coincidental and irreversible behaviour in both states. Concentration dependent amyloid fibril formation was confirmed by Thioflavin T and Congo Red binding and its morphology was studied by transmission electron microscopy (TEM). This is the first report on biophysical characterization of folding intermediates of LBTI and its aggregation behaviour to the best of our knowledge.

1. Introduction

Natural inhibitors are generally divided into 18 families, serine protease Bowman-Birk-type protease inhibitors (BBIs) are one among them. LBTI belongs to the bifunctional BBIs that consist of symmetrically arranged trypsin- and chymotrypsin-binding subdomains. Trypsin inhibitor from LBTI has been purified and characterized [1]. Purification, crystallization, and preliminary x-ray studies of LBTI have been done [2]. It is 9.0 kDa monomer having 83 residues among which 57 residues matches BBI sequences. It has 20% β sheet structure with 6 β-strands and 7 disulfide bonds, but devoid of free cysteine (–SH). The only tyrosine residue (Tyr-69) resides between two disulfide bonds (cys68-cys22 and cys72-cys18), resulting a rigid constrained structure. BBIs are small and cysteine-rich serine protease inhibitors with molecular mass 6–20 KDa. They are widespread in monocotyledonous and dicotyledonous plants, particularly in leguminous seeds. Because of its high thermostability and inhibitory activity, it is widely used in biochemical procedures [3]. The active site in all BBIs has a common fold consisting of two distinct sub-domains with a β-hairpin and an antiparallel β sheet structure, stabilized by disulfide bonds. The loops are generally very rigid. The most unusual feature of BBI structures are the presence of exposed hydrophobic patches and lack of any hydrophobic core, unlike globular proteins. The exposed hydrophobic patches predominant in sub-domain 2 seem to be responsible for self-association of the inhibitor. The LBTI molecule adopts a 'bow-tie' fold canonical to the Bowman-Birk protease inhibitor family. The dimeric state is stabilized by a set of hydrogen bonds and a hydrophobic core [4].

Most of the BBIs tend to form homo or hetero- dimers, trimers and more complex oligomers. Some studies indicate the pivotal role

Abbreviations: LBTI, Lima Bean Trypsin Inhibitor; MG, molten globule; PPI, protein protease inhibitor; PI, protease inhibitor; I^a, amyloidiogenic intermediate; Y69, tyrosine 69; E70, glutamate 70; GdnHCl, guanidine hydrochloride; TEM, transmission electron microscopy; CD, circular dichroism.

* Corresponding authors.
E-mail addresses: javedjmk@gmail.com, jmkhan@ksu.edu.sa (J.M. Khan), sfatima1@jmi.ac.in, amu.jmi@rediffmail.com (S. Fatima).

http://dx.doi.org/10.1016/j.ijbiomac.2017.05.040
0141-8130/

of charged interactions in the case of monmer/dimer equilibrium [5]. The absence of hydrophobic core and high content of disulfide bonds result in a constrained conformation that may responsible for the remarkable stability exhibited by BBIs [6].

Protease inhibitors (PIs) like angiotensin-converting enzyme inhibitors (ACEIs) form the first-line pharmacotherapy for heart failure [7]. Metalloproteases and their endogenous inhibitors TIMPs (tissue inhibitor of metalloproteinases), regulate downstream signaling of the tumor necrosis factor receptor and the interleukin-6 receptor, epidermal growth factor receptor and Notch, which are all pertinent for inflammatory responses [8]. The launch of first-generation PIs was a major step forward in Hepatitis C Virus treatment, while the development of second-generation PIs yields higher antiviral potency, more convenient daily administration, fewer side effects and potential activity against resistance-associated variants [9]. The human immunodeficiency virus type 1 protease enzyme (HIV-1 PR) is one of the most important targets of antiretroviral therapy used in the treatment of AIDS patients and it has been area of active research [10]. Protease inhibitors have been investigated for their potential in cancer therapy [11]. PI can both be chemicals or proteins, with more safety associated with the use of protein protease inhibitor as drug. Proteases and their natural protein inhibitors are among the most intensively studied protein–protein complexes [12]. A novel anti-hyperglycemic agent (teneligliptin) that is peptidase inhibitor has been developed for long-term efficacy and safety in patients with type 2 diabetes [13]. Considering widespread applications of PPI, active research to understand their structure, function and stability are required. PPI have been purified and characterized from a large number of sources, ex- Soybean, Peanut, Potato, wheat etc [14].

For any protein to be functional, it has to be folded to its native conformation. With the view to understand folding of proteins, "Folding funnel" landscape model has been suggested according to which proteins fold to the native state through any of a large number of pathways and intermediates [15]. Proteins normally fold via a number of intermediates, in order to attain their unique native conformation [16]. Characterization of folding intermediates may unravel the mystery of the steps involved in the proper folding of proteins. Describing the structures of intermediates along the folding landscape is of key importance to comprehend the folding reaction or to design new proteins [17]. Also many diseases of genetic nature are coupled with protein misfolding due to formation of stable, non-functional intermediate species of the protein [18]. The Molten Globule (MG) is a highly dynamic intermediate with native-like secondary structure but loose tertiary structure [19]. A number of studies are done to characterize molten globule states of different proteins in an attempt to understand unfolding pathways of proteins.

Keeping in view importance of PI and absence of enough work done on their folding pathways, in this paper we have tried to characterize folding intermediates of LBTI under different denaturation conditions. From the spectroscopic results, it was observed that LBTI forms molten globule structure at pH 2 and post-molten globule state at pH 4 that is very prone to form aggregates; denoted as I^a.

2. Materials and methods

2.1. Materials

LBTI, ThT, Congo Red, ANS and GdnHCl were purchased from Sigma Chemical Co. (St. Louis, MO, USA). All other reagents and buffer compounds used were of analytical grade.

LBTI stock solution (5 mg ml^{-1}) was prepared in 20 mM sodium phosphate buffer pH 7.4 and LBTI was 17 times diluted in different pH buffers. Experiments were carried out in 20 mM of the following buffers: pH 0.6–2.8 Glycine-HCl buffer, pH 3–5 Sodium acetate buffer, pH 6–7.4 Sodium phosphate buffer. 6 M GdnHCl solutions were prepared in 20 mM sodium phosphate buffer, pH 7.4. pH measurements were carried out on an Mettler Toledo pH meter. Protein concentrations were determined with Lowry method. LBTI was incubated for 12 h at desired pH before spectroscopic measurements.

2.2. Circular dichroism (CD) measurements

CD measurements were carried out with a Jasco spectropolarimeter model J-815, equipped with a microcomputer. The instrument was calibrated with (+)-10-camphorsulfonic acid. All the CD measurements were carried out at 25 °C with a thermostatically controlled cell holder attached to a Neslab RTE-110 water bath with an accuracy of +0.1 °C. For pH and GdnHCl denaturation, the far-UV CD spectra were measured with a protein concentration of 0.3 mg ml^{-1} and 1 mm path length.

For aggregation study, the increasing concentrations of LBTI (0.3, 1.0 and 5.0 mg ml^{-1}) were incubated overnight. Aggregated samples spectra were collect in the range of 200–250 nm.

2.3. Fluorescence measurements

Intrinsic fluorescence was executed on a Shimadzu spectrofluorometer, model RF-540. The fluorescence spectra were measured at a protein concentration of 0.3 mg ml^{-1}. Intrinsic spectra were recorded between 300 to 400 nm with excitation wavelength of 280 nm.

50 times more ANS was added compared LBTI in a working solution. ANS spectra were scanned in the range of 400–600 nm with excitation at 380 nm. The LBTI concentrations were used 0.3 mg ml^{-1} in both the measurements.

2.4. Turbidity measurements

Turbidity of LBTI at pH 4.0 was measured by Perkin Elmer double beam UV–vis spectrophotometer, Lambda 25 in a cuvette of 1 cm path length. The different concentrations (0.3–10.0 mg ml^{-1}) of LBTI were incubated at pH 4.0 for overnight and turbidity was measured at 350 nm.

2.5. Thioflavin T (ThT) assay

The ThT was dissolved in double distilled water and filtered with a 0.2 μm Millipore syringe filter. The stock a concentration of ThT was calculated by using extinction coeficent 36,000 M^{-1} cm^{-1} at 412 nm [20]. LBTI was incubated in the different concentration from 0.3 to 10.0 mg ml^{-1} for overnight in 20 mM sodium acetate buffer at pH 4.0. Overnight incubated samples were further mixed with 15 μM of ThT solution and again incubated for 30 min in the dark. The fluorescence of ThT was excited at 440 nm and spectra were recorded from 460 to 600 nm. The excitation and emission slit widths were fixed at 10 nm. Samples spectra were further subtracted from an appropriate blank.

2.6. Congo Red (CR) dye binding

The CR was prepared in double distilled water and filtered through 0.2 μm Millipore syringe filter for further use. The CR concentration was estimated by using extinction coeficent 45,000 M^{-1} cm^{-1} by taking absorbance at 498 nm [21]. The different concentrations of LBTI were incubated in 20 mM sodium acetate

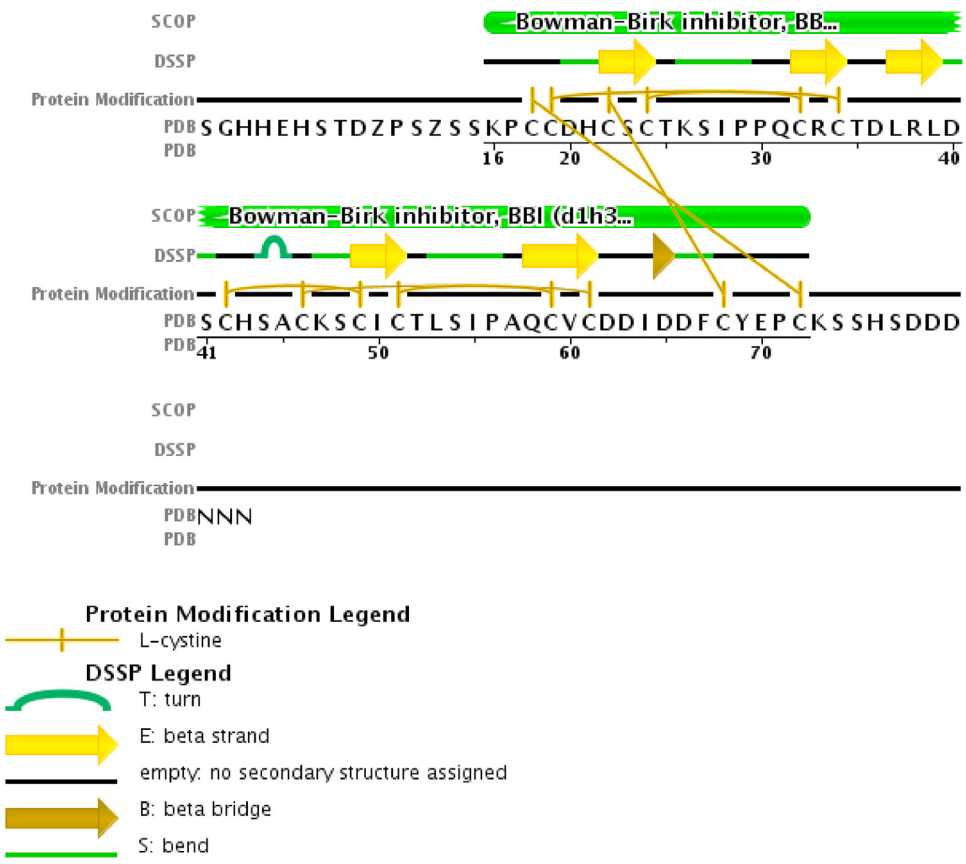

Fig. 1. Graphical representation of LBTI sequence.
Graphical presentation following crystal structure of LBTI (PDB 1H34) from http://www.rcsb.org/pdb/explore.do?structureId=1h34. Tyrosine at 69th position is indicated with a red upward arrow. SCOP: Domain annotation from the SCOP database. DSSP: Secondary structure assignment. PDB: Protein sequence from the PDB database.

buffer at pH 4.0 for overnight incubation. The incubated samples were further incubated with CR (15.0 μM) and kept for 15 min at room temperature in dark. The absorbance spectra of samples in the wavelength range of 300–900 nm were recorded with a UV–vis spectrophotometer (Perkin Elmer Lambda 25) in a 1 cm path length cuvette. The absorbance spectra of blank (without CR) were also taken in same wavelength range. The control spectra were further subtracted from aggregated samples with CR and subtracted spectra were plotted.

2.7. Transmission electron microscopy (TEM)

JEOL transmission electron microscopy was used to take amyloid image by applying voltage of 200 kV. Fibril formation was evaluated by pouring 6 μl of protein sample (2.0 and 5.0 mg) on 200-mesh, copper grid covered by carbon-stabilized Formvar film. Excess of liquid was eliminated after 5 min and then grids were negatively stained with 2% (w/v) uranyl acetate. Images were taken at 10 000× magnification.

3. Results

3.1. Acid-induced unfolding of LBTI

When the proteins are highly charged at extremes of pH, strong electrostatic repulsions trigger partial denaturation of protein [22]. Far-UV CD spectra at different pH are shown in Fig. 2A and comparative change in secondary structure versus pH is shown in Fig. 2B. CD spectra of LBTI at pH 7 shows negative peak at 208 nm (Fig. 2A) as consistent with β-strands crystal structure [23]. Secondary structure of LBTI was retained over entire range of pH 3–7 (Fig. 2A & B). Below pH 1, CD value has decreased slightly, but the protein has lost its structure completely with 6 M GdnHCl. The far-UV CD results are suggesting that LBTI secondary structure remain stable in the pH range of 1–7.

3.2. Tertiary structural change

C18-C72 and C22-C68 cystines provide a rigid environment around Y69, only steric changes are allowed around such constrained structure (Fig. 1) [24]. Y69 is the only residue in LBTI that could be excited at 280 nm and emitted near 334 nm. This might explain low fluorescence signal given by LBTI at pH 7 (Fig. 3A). A drop in intrinsic fluorescence intensity (Fig. 3B) was observed when pH was lowered, could be explained by change in conformation of protein with the changing pH. The blue-shifted λ_{max} (Fig. 3C) suggests pH-induced change that resulted in decreased polarity around Tyr residue. The shift in wavelength maximum was suggested that the tertiary structure of LBTI was disrupted at lower pH.

The exposure of hydrophobic residues was further checked by ANS fluorescence. ANS fluorescence enhances substantially upon binding to exposed hydrophobic surfaces. Hence, ANS is a hydrophobic fluorescent dye that reports folding status of a protein and peptides [25]. Fluorescence spectra of LBTI-ANS complex at pH 7–2 shown in Fig. 4A. From the figure, it was found that the ANS fluorescence spectra at pH 2.0 is blue shifted along with increase in fluorescence intensity compared to pH 7. In Fig. 4B, ANS fluorescence intensity at 485 nm has been plotted against pH. The fluorescence intensity is increasing with respect to acidity of medium. The wavelength maximum of ANS with native LBTI exhib-

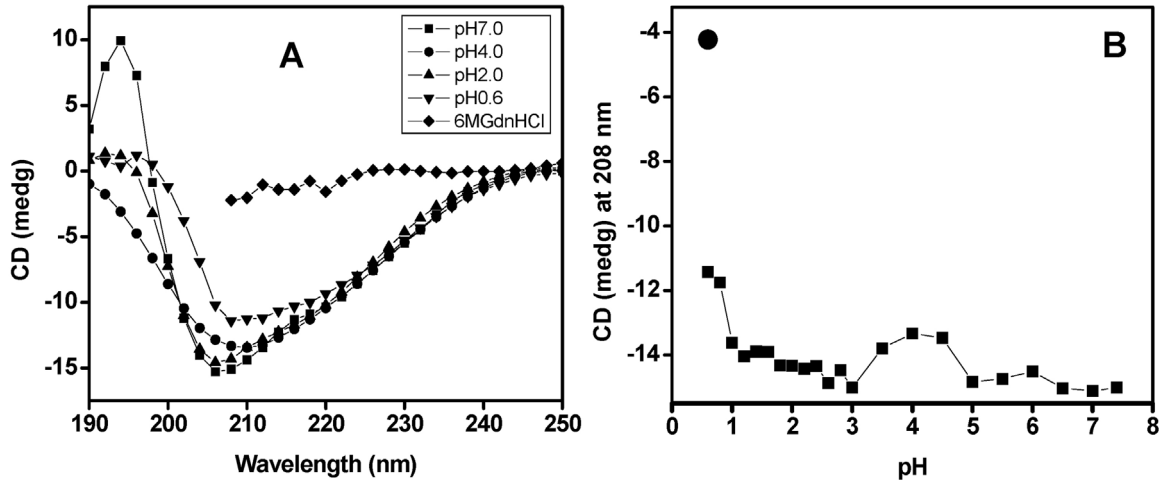

Fig. 2. pH induced secondary structural change of LBTI.
(A) Far-UV CD spectra of PPI at pH 7 (-■-), pH 4 (-●-), pH 2 (-▲-), pH 0.6 (-▼-) and 6 M GdnHCl (-♦-). (B) The change in elipticity of LBTI at 208 nm was plotted with respect to pH. LBTI was incubated at different pH for overnight prior to measurements. All the samples were incubated at different 20 mM pH buffers for overnight. The LBTI concentration was 0.3 mg ml^{-1} in all the samples.

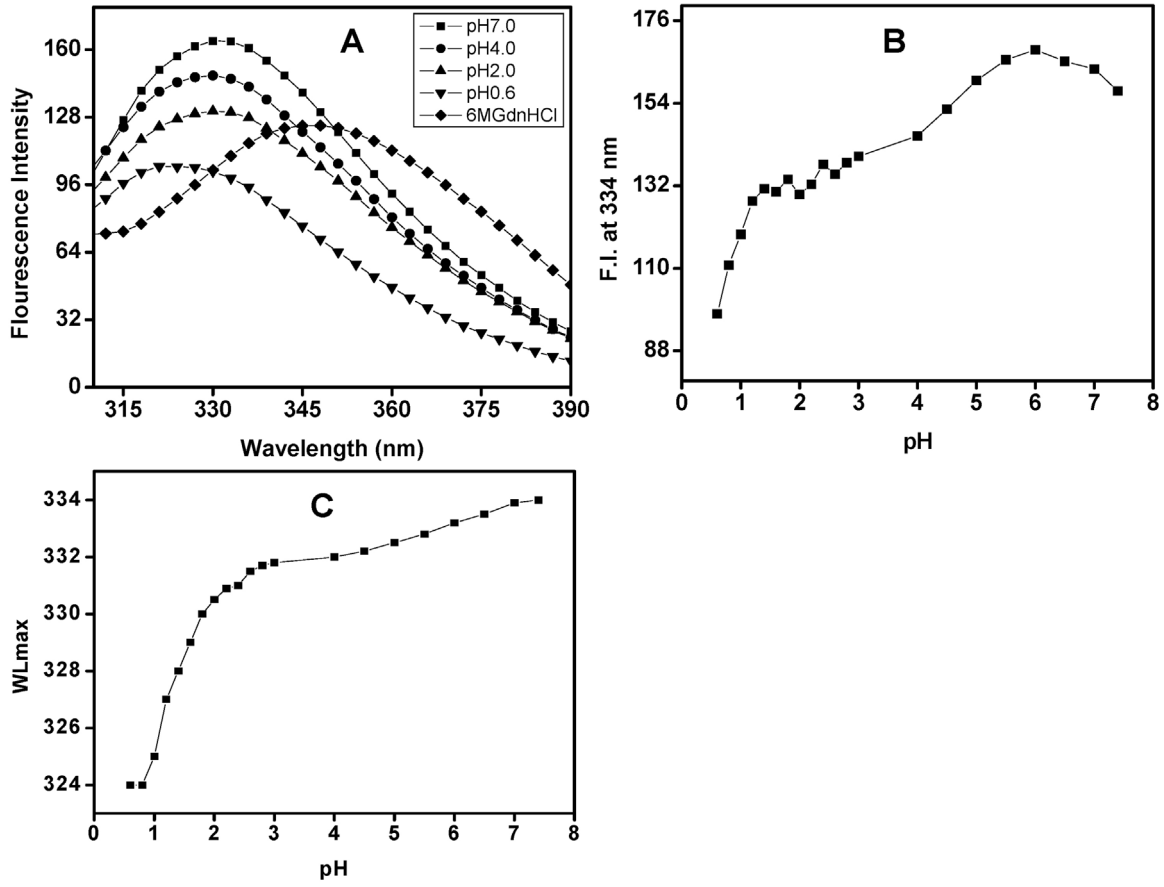

Fig. 3. Tertiary structural changes were measured by intrinsic fluorescence.
LBTI concentration was 0.3 mg ml^{-1} in all the samples. (A) Fluorescence emission spectra of LBTI at pH 7 (-■-), pH 4 (-●-), pH 2 (-▲-), pH 0.6 (-▼-) and in the presence of 6 M GdnHCl (-♦-). (B) Changes in relative fluorescence intensity (RFI) at 335 nm of LBTI at different pH. (C) The wavelength maxima of LBTI were plotted with respect to pH. Spectra were obtained by exciting at 280 nm.

ited maximum emission around 505 nm which was decreased to 480 nm at pH 2 (Fig. 4C) suggesting high binding of ANS at lower pH.

If we observe further details, no significant change was observed in Y69 emission spectrum or LBTI-ANS binding emission spectrum in the pH 7–6 (Fig. 5A). In the range of pH 6–4, a sudden single step blue shift (505 nm to 480 nm) in ANS binding was observed (Fig. 4C), with a small 3 nm blue shift (334 nm to 332 nm) in Y69 emission spectrum (Fig. 3C). Upon decrease in pH below 4, LBTI-ANS complex didn't register any further drop in emission

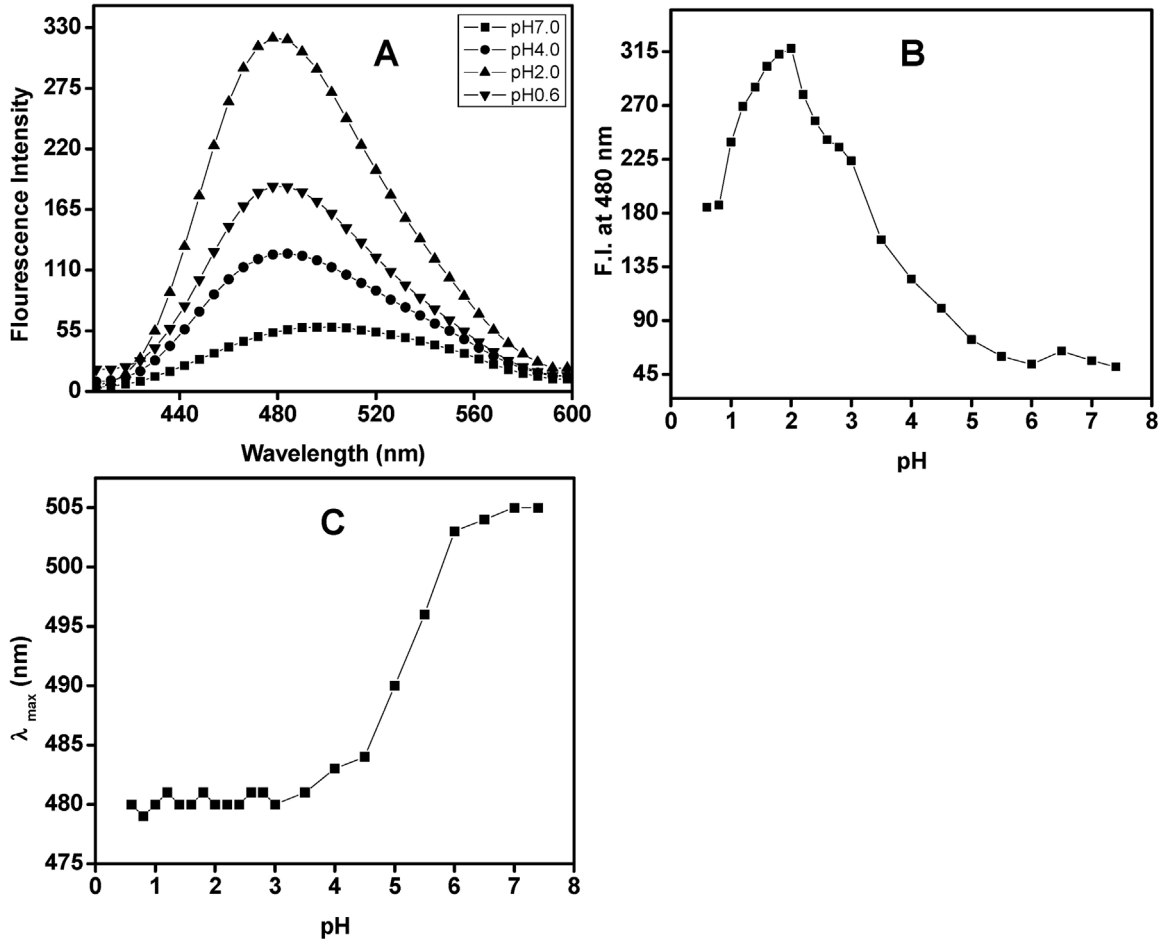

Fig. 4. Change in chromospheres position was monitored by ANS dye binding.
(A) Extrinsic fluorescence spectra of LBTI at pH 7 (-■-), pH 4 (-●-), pH 2 (-▲-) and pH 0.6 (-▼-). (B) pH dependant changes in ANS fluorescence intensity of LBTI at 480 nm. (C) Change in wavelength maximum of LBTI was plotted verses pH. Prior to measurements all the samples were incubated for 12 h in a 20 mM respective pH buffer with 0.3 mg ml^{-1} LBTI concentration and 50 times more ANS were added in all the samples.

spectrum wavelength, but in case of Y69 a significant drop of emission wavelength (334 nm–324 nm) has been reported between pH 4–pH 1 along with drop of fluorescence intensity (Fig. 3B). LBTI lacks hydrophobic core and hydrophobic patches are solvent exposed. The blue shift of LBTI-ANS emission spectrum indicates increase in protein-ANS binding and/or withdrawal of hydrophobic patches from solvent. Increase in protein-ANS fluorescence intensity further supports increment in protein-ANS binding. Along with hydrophobic patches, cationization of side-chains may have helped in increased binding with anionic ANS salt with decrease in pH [26]. Blue shift in the range of pH 4–1 with decrease in fluorescence intensity, suggests shifting of Y69 from polar to non-polar and less solvent accessible environment. As the blue shift registered in Y69 emission spectrum below pH 4, followed by abrupt blue shift in ANS emission spectrum, it seems decrease in pH may have affected the citrate shielding of E70 on Y69 in a way that it may have pushed to a nonpolar pocket, without any reported change in 2° structure (Fig. 2).

A significant alteration of tertiary structure at pH 2 with insignificant change in secondary structure designated the formation of molten globule-like structure. Another important state was observed at pH 4, with no change of secondary structure (Fig. 2), altered tertiary contacts (Fig. 3) and less exposed hydrophobic patches than that of pH 2 (Fig. 4). We have termed this as I^a state of LBTI, a state which can be observed between MG state and native state.

The unfolding mechanism of LBTI can be described using a Linear Three-State Scheme:

$$\underset{\text{atpH7}}{\text{NativeState}} \rightarrow \underset{\text{atpH4}}{\text{I}^a} \rightarrow \underset{\text{atpH12}}{\text{MGstate}}$$

3.3. Chemical stability of LBTI in native and molten globule states

GdnHCl, is a well known protein denaturing salt, becomes a base with a stable +1 charge at physiological pH [27]. Most of the proteins have reported GdnHCl dependent unfolding [28]. The secondary structure study has been done on the basis of CD ellipticity at 208 nm that shows the resultant structure of all 6 β-sheet strands present in LBTI, thus gives a global view of the protein. In contrary, the tertiary structure study has been done on the basis of a lone tyrosinyl residue Y69 that resides towards the C-terminus of LBTI that can report only a local conformation of the protein. Even though urea and GdnHCl both are presumed to bind to peptide bonds, the polypeptide unfolding capacity of GdnHCl is substantially higher than urea [29]. Studies on coiled coils by Monera et al. (1994) and Grigoryan and Keating (2008) suggested that electrostatic interactions have no effect on GdnHCl induced unfolding. In solutions, GdnHCl ionizes to Gdn(+) and Cl(−) ions that neutralizes the positively and negatively charged amino acid side chains of the proteins hence reducing or completely eliminating any stabilizing or destabilizing electrostatic interactions [30].

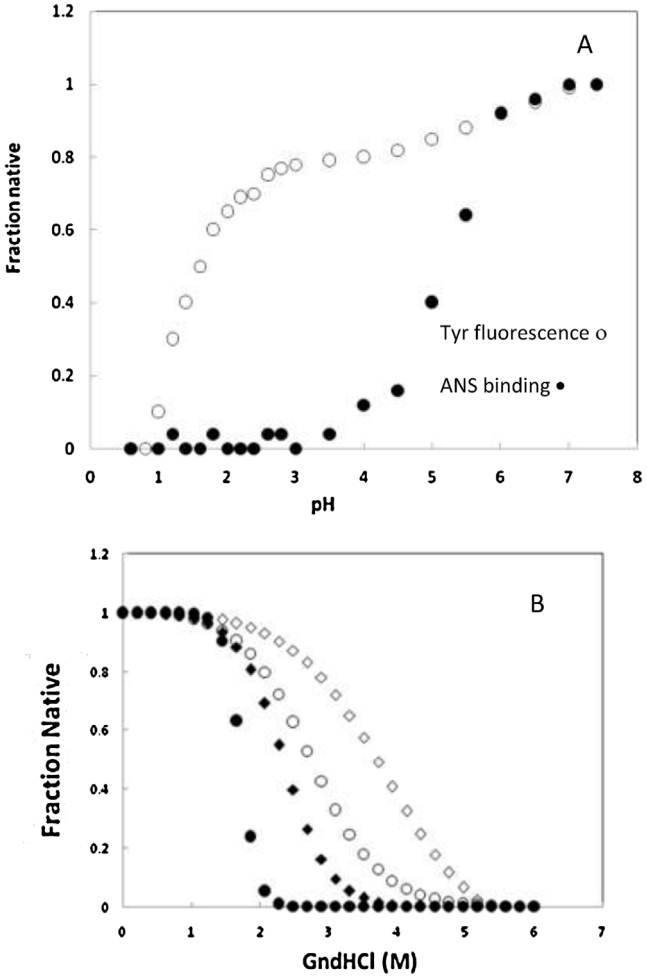

Fig. 5. (A) Tertiary structure change of LBTI as fraction of native state against pH. pH-induced unfolding of LBTI monitored by emission wavelength maxima (○) after exciting at 280 nm (Tyr fluorescence) and fluorescence maxima (●) by ANS binding after exciting at 480 nm. LBTI concentration was 0.3 mg ml^{-1} in all samples. (B) GdnHCl-induced denaturation of LBTI was monitored by changes in secondary and tertiary structure. GdnHCl-induced unfolding of LBTI at pH7 (◊) and pH 2 (○) as fraction native state monitored by change in fluorescence emission intensity at 335 nm plotted as a function of GdnHCl concentration after excitation at 280 nm (for tertiary structure) and at pH7 (♦) and pH 2 (●) monitored ellipticity measurement at 222 nm by far UV-CD (for secondary structure). LBTI concentration was 0.3 mg ml^{-1} in all the samples.

GdnHCl induced denaturation showed sigmoidal, non-coincidental and irreversible transitions in both states (Fig. 5B). Non-coincidence is a characteristic for existence of possible folding intermediate state. While studying GdnHCl denaturation of human placental cystatin (HPC), a low molecular weight thiol proteinase inhibitor (12.5 kDa) intermediates or non-native states were observed at lower concentrations of denaturant [28]. The global secondary structure seems more susceptible to GdnHCl denaturation (Cm are 2.34 M and 1.72 M at pH 7 and 2 respectively) than local tertiary structure (Cm are 4.08 M and 2.73 M at pH 7 and 2 respectively) around Y69, and both level of structures are more susceptible at pH 2 in comparison to pH 7 (Table 1). No change in secondary or tertiary structure has been observed in the presence

Table 1
Cm of secondary and tertiary structure of LBTI at pH 7.0 and pH 2.0.

Cm	pH 7.0	pH 2.0
2° structure ($CD_{208\,nm}$)	2.34 M	1.72 M
3° structure ($Em_{335\,nm}$)	4.08 M	2.73 M

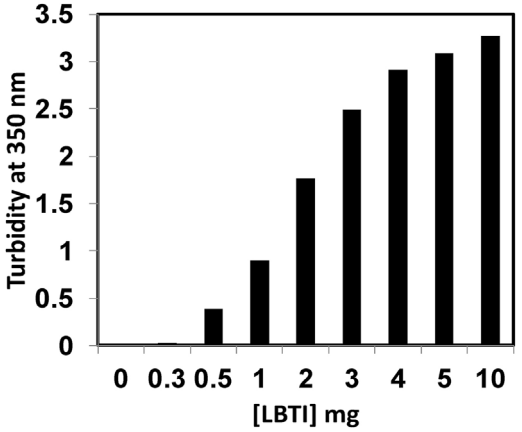

Fig. 6. Turbidity of the samples was measured to detect aggregation in solution. Turbidity was measured at different concentration of LBTI by taking absorbance at 350 nm in 20.0 mM sodium acetate buffer pH 4.0 at 25 °C. Before measurements all the samples were incubated overnight.

of 0–1 M GdnHCl. The complete secondary structure loss took place with 2 M and 4 M GndHCl at pH 2 and pH 7 respectively. On the other hand, the tertiary structure change under GdnHCl denaturation seems much rigid, due to the presence of C18-C72 and C22-C68 cystines around Y69.

3.4. Characterization of aggregated state of LBTI

An aggregating intermediate state is appearing at pH 4. LBTI is a monomer at native state, but concentration and pH dependant oligomerization takes place. With decrease in pH from pH 7 to pH 4, the internalization of hydrophobic patches and an optimum ion-pairing may have provided a suitable environment for aggregation of LBTI (Fig. 4). On further decrease in pH, around pH 2; the high cationic repulsion seems play a role in absence of aggregation.

Many proteins form amyloid fibril with respect to change in pH. The amyloid fibril formation of ABri peptides depend on pH of the solutions [31]. In this study, we have tried to characterize the amyloid fibril formation in the pH range from 0.6 to 7.4. LBTI was not forming amyloid fibril in the whole pH range except at pH 4.0. The amyloid fibril formation of LBTI was confirmed by various spectroscopic techniques.

3.5. Turbidity measurements

Turbidity of samples can be measured in the near UV range mostly at 350 nm. The aggregated samples become more turbid and optical density will increase. We have monitored the aggregate formation in LBTI with respect to change in protein concentrations from 0.3 to 10.0 mg ml^{-1} at pH 4.0 by taking optical density at 350 nm. As can be seen from Fig. 6, the optical density at 350 nm of LBTI was gradually increased in the concentrations of LBTI 0.5–10.0 mg and maximum turbidity was recorded at 10.0 mg of LBTI concentration while at 0.3 the turbidity is almost negligible. From the turbidity results, it can be concluded that the aggregation of LBTI was dependent on the concentrations of LBTI and pH, the LBTI was not forming any aggregate at low as well high pH even in the presence of low and high concentrations of proteins. Similar aggregates were also seen in pepsin which forms aggregate at neutral pH and room temperature [32].

3.6. Thioflavin-T dye binding

From the turbidity observations, it was confirmed that LBTI become aggregated at pH 4.0 in the concentrations range of

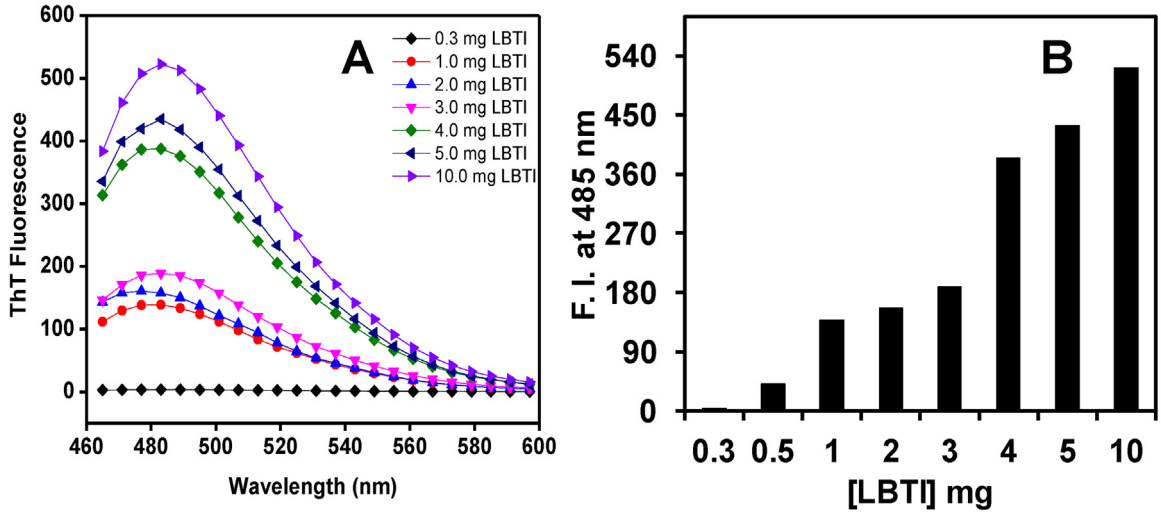

Fig. 7. Amyloid fibril formation in LBTI was measured by ThT fluorescence. ThT fluorescence spectra at pH 4.0 in different concentration 0.3 (-♦-), 1.0 (-●-), 2.0 (-▲-), 3.0 (-▼-), 4.0 (-♦-), and 5.0 (-◀-) 10.0 (-▶-) mg ml^{-1} of LBTI. (B) The effect of varying concentration of LBTI at pH 4.0 on amyloid fibrillogenesis was measured by ThT fluorescence intensity at 485 nm after excitation at 440 nm.

0.5–10.0 mg. Now it was further confirmed whether these aggregated samples were amorphous or have an amyloid-like structures. For this, we have performed ThT dye binding assay. ThT, a benzothiazole dye; usually binds and forms a highly fluorescent complex with amyloid or amyloid-like fibrils [33]. ThT binds various fibrils such as exposed β-sheet edges, an extended β-sheet surface, as well the laminated "steric zipper" interface between the β-sheets and cross-β sheet architecture [34]. The ThT fluorescence spectra of aggregated and non aggregated samples are shown in Fig. 7A. A huge increase in ThT fluorescence intensity was noticed in the concentration range of 1.0–10.0 mg where as at 0.3 mg concentration insignificant ThT binding was found. At low concentrations of LBTI, the fluorescence intensity is found low while at higher LBTI concentrations the quantum yield of fluorescence intensity is found very high. We further plotted the ThT fluorescence intensity at 485 nm at different concentrations of LBTI at pH 4.0 which are shown in Fig. 7B. The LBTI protein was showing enhanced ThT fluorescence intensity in the concentration range of (0.5–10.0 mg) at pH 4.0 and maximum fluorescence intensity was recorded at 10.0 mg and no ThT binding taking place at 0.3 mg LBTI concentrations. The ThT dye binding results revealed that LBTI protein form amyloid fibril in the concentration range of 0.5–10.0 mg at pH 4.0. However, at higher and lower pH fibril formation was not taking place. ThT fluorescence results of LBTI suggest that pH dependent aggregates have amyloid fibril like structures.

3.7. Congo Red (CR) dye binding assay

Sometimes ThT binds to the multimer of proteins at native condition. To overrule this problem, we performed a CR binding assay to confirm the amyloid fibril formation in LBTI at different concentrations at pH 4. CR is known to bind to the cross β-sheet structure of proteins [35]. The CR binding results are shown in Fig. 8. The dye binding to protein in the absence of aggregates showed a maximum absorbance at 495 nm. However, at higher concentrations when aggregates are formed, the absorbance maxima were red shifted to around 572 nm at pH 4.0. Due to CR binding now it is confirmed that the LBTI was forming amyloid-like structure at higher concentrations at pH 4 only. pH induced unfolded states that are prone to aggregation forming amyloid-like fibrils have been reported in Pancreatic thiol proteinase inhibitor- a protease inhibitor isolated from pancreas of *Capra hircus* [36].

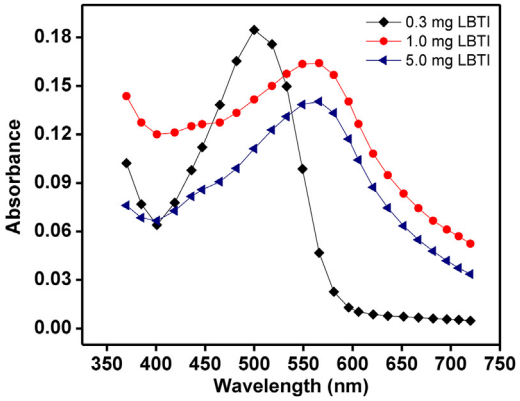

Fig. 8. Amyloid fibril formation in LBTI was measured by Congo red binding. The absorbance spectra of LBTI obtained from Congo red binding assay at pH 4.0 with different protein concentration 0.3 (-♦-), 1.0 (-●-) and 5.0 (-◀-) mg ml^{-1} of LBTI.

3.8. Far-UV CD spectroscopy results

Far-UV CD spectroscopy study was performed to determine the change in secondary structural contents of protein upon aggregation. From Fig. 9, far-UV CD spectra of LBTI (0.3 mg ml^{-1}) at pH 4.0 exhibited single minima at 208 nm which is suggesting that LBTI has a β-strand as a secondary structure as discussed above. The peak of LBTI at 208 nm, transformed into a single peak at higher wavelength around 225–230 at higher concentration of LBTI (1.0 and 5.0 mg ml^{-1}). The peak centered at 225–230 nm could be amyloid specific CD signature. The higher intensity and the red shift of the signal at higher concentrations may reflect decreased solvent accessibility upon aggregation [37].

3.9. TEM results

Finally, to confirm morphology of LBTI peptides aggregates, TEM was used to distinguish the morphology of aggregates. TEM has been routinely employed to characterize the shape and size of protein aggregates [38,39]. The two different concentrations of LBTI were showing amyloid-like aggregates at pH 4.0, as can be seen in Fig. 10. LBTI formed small amyloid structure at 2.0 mg ml^{-1} concentration while at 5.0 mg ml^{-1} concentration bigger sized amyloid formed. The bigger size amyloid fibril formation indicated the

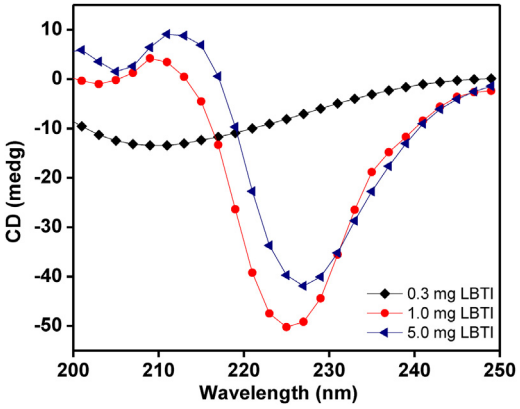

Fig. 9. Secondary structural changes monitored by Far-UV CD.
Far-UV CD spectra of LBTI at different concentrations 0.3 (-♦-), 1.0 (-●-) and 5.0 (-◀-) mg ml^{-1} of LBTI at pH 4.0.

power of interactions that stabilized these structures [40]. It is also believed that large amyloid formed through the lateral joining of smaller amyloid [41]. From the ThT and CR binding as well as TEM results it could be concluded that LBTI is forming amyloid at pH 4.0. The amyloid fibril formation is also dependent on the concentrations of LBTI.

4. Discussion

In this study, we have characterized two important partially folded states of LBTI; an MG state at pH 2.0 with native like secondary structure and altered tertiary structure. As compared to native state, reduced fluorescence intensity along with blue shift in wavelength maxima are important characteristics of MG state. Similar findings with reduced fluorescence signal in acid-induced MG state have been attributed to presence of charged amino-acid residues nearby Trp 104, in case of alpha-lactalbumin [42]. The MG state may have exposed hydrophobic patches as observed by binding of ANS, a hydrophobic cluster binding dye. The MG state of LBTI lacks enzymatic activity (data not shown). MG state of Cicer α-galactosidase with enhanced binding of ANS at pH 2.0, lack of activity but retained significant secondary structure has been reported [43]. Further, GdnHCl induced denaturation of native and MG state study revealed that native state is evidently more stable than MG state. Chemical agents like GdnHCl are often used to compare stability of proteins and their conformational states. Also, the presence of sigmoidal, non-coincidental transition curves may signify presence of additional intermediate states [44]. The evident rigidity reflected by GdnHCl denaturation of a local tertiary structure in comparison to secondary structure indicates the presence of a rigid cystine-rich motif around the lone fluorophores Y69 that resides towards C-terminal end of LBTI monomer.

Induction of a low pH-induced MG state which may be triggered by the disruption of key salt bridges in proteins has been reported frequently [45,46]. The relevance of partially ordered states of proteins (such as the MG state) in cellular processes is beginning to be understood [47]. It is postulated that the structural folding of protein annexin and a malarial protein at low pH, could explain how a soluble protein may undergo transition into a molecule able to penetrate the membrane hydrophobic region [48,49]. Human breast cells in culture (MCF-7) transfected with p53-GFP revealed localization of p53 in acidic vesicles, suggesting that the low pH conformation is present in the cell and p53 may play physiological or pathological roles in acidic microenvironments [50].

Biological significance of acid-induced states that are prone to oligomerisation or aggregation has been recently realized. It is argued that the specific conformation of the acid-induced state of PrP^C would provide crucial insights into the mechanisms of oligomerization and further pathogenic conversion as well as facilitating the design of novel medical chaperones for treating prion diseases [51]. One such acid-induced partially folded state that is prone to aggregation has been reported in this study. LBTI is not prone to aggregation in the entire pH range except at pH 4.0, close to its theoretical pI (pH 5.0). Amyloidogenic intermediate (I^{amy}) at pH 4.0 showed concentration-dependant increase in turbidity measurement experiments. This result was further confirmed by ThT and Congo-Red binding, dyes used as probe for fibril formation. TEM images also showed formation of fibrils in concentration dependant manner. This may be the first report on characterization of folding intermediates of LBTI as per our knowledge.

Acknowledgements

The authors extend their appreciation to the Deanship of Scientific Research and the Research Center, College of Pharmacy, King Saud University for funding this research.

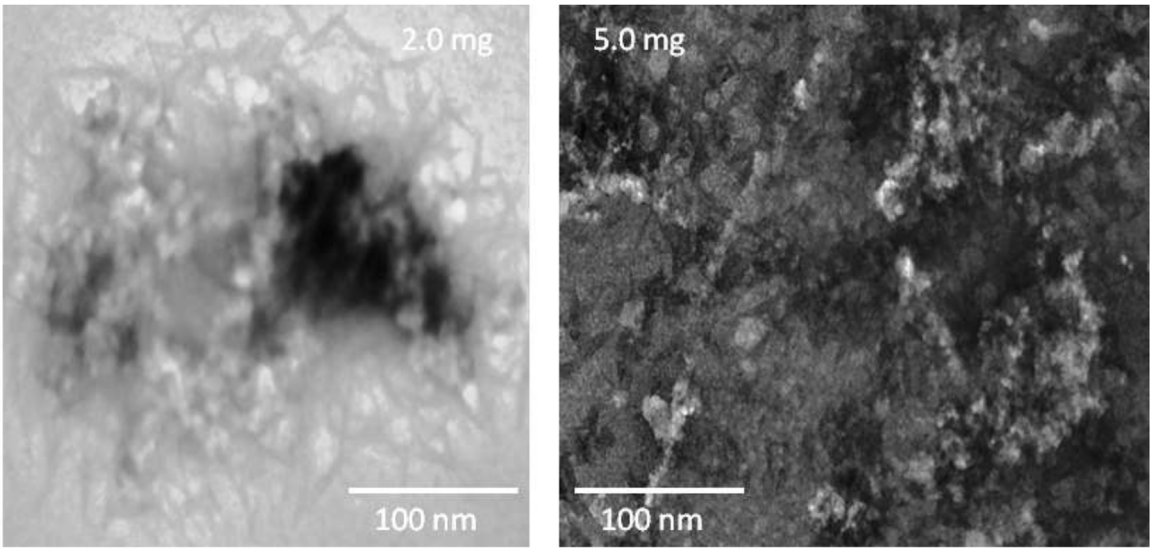

Fig. 10. TEM images. Morphology of LBTI aggregates was visualized by TEM at two representative concentrations (A) 2.0 mg and (B) 5.0 mg at pH 4.0.

References

[1] G. Jones, S.H. Moore, Properties of chromatographically purified trypsin inhibitors from lima beans, J. Biochem. 2 (1963) 66–71.
[2] C. Samudzi, S. Schroeder, S. Griffith, X. Chen, T.P. Quinn, Crystallization and preliminary studies of Lima bean trypsin inhibitor, Proteins 27 (1997) 311–314.
[3] Y. Birk, Lima bean trypsin inhibitors, Methods Enzymol. 45 (1976) 707–709.
[4] J.E. Debreczeni, G. Bunkóczi, B. Girmann, G.M. Sheldrick, In-house phase determination of the lima bean trypsin inhibitor: a low-resolution sulfur-SAD case, Acta Crystallogr. D Biol. Crystallogr. 59 (2003) 393–395.
[5] K.N. Rao, C.G. Suresh, Bowman-Birk protease inhibitor from the seeds of Vigna unguiculata forms a highly stable dimericstructure, Biochim. Biophys. Acta. 1774 (10) (2007) 1264–1273.
[6] R.R. Singh, A.G. AppuRao, Reductive unfolding and oxidative refolding of a Bowman-Birk inhibitor from horsegram seeds (Dolichosbiflorus): evidence forhyperreactive disulfide bonds and rate-limiting nature of disulfide isomerization in folding, Biochim. Biophys. Acta 1597 (2) (2002) 280–291.
[7] H. Krum, A. Driscoll, Management of heart failure, Med. J. 199 (2013) 334–339.
[8] R. Khokha, A. Murthy, A. Weiss, Metalloproteinases and their natural inhibitors in inflammation and immunity, Nat. Rev. Immunol. 13 (2013) 649–665.
[9] J.A. Ilyas, J.M. Vierling, An overview of emerging therapies for the treatment of chronic hepatitis C, Med. Clin. North. Am. 98 (2014) 17–38.
[10] D.A. Antunes, M.M. Rigo, M. Sinigaglia, R.M. de Medeiros, D.M. Junqueira, S.E. Almeida, G.F. Vieira, New insights into the in silico prediction of HIV protease resistance to nelfinavir, PLoS One 9 (2014) e87520.
[11] R.B. Batchu, O.V. Gruzdyn, C.S. Bryant, A.M. Qazi, S. Kumar, S. Chamala, S.T. Kung, R.S. Sanka, U.S. Puttagunta, D.W. Weaver, S.A. Gruber, Ritonavir-mediated induction of apoptosis in pancreatic cancer occurs via the RB/E2F-1 and AKT pathways, Pharmaceuticals (Basel) 7 (2014) 46–57.
[12] J. Otlewski, F. Jelen, M. Zakrzewska, A. Oleksy, The many faces of protease-protein inhibitor Interaction, EMBO J. 24 (2005) 1303–1310.
[13] M. Goda, T. Kadowaki, Teneligliptin for the treatment of type 2 diabetes, Drugs Today (Barc.) 49 (2013) 615–629.
[14] E. Poerio, S. Di Gennaro, A. Di Maro, F. Farisei, Primary structure and reactive site of a novel wheat proteinase inhibitor of subtilisin and chymotrypsin, Biol. Chem. 384 (2003) 295–304.
[15] P.E. Leopold, M. Montal, J.N. Onuchic, Protein folding funnels: a kinetic approach to the sequence-structure relationship, Proc. Natl. Acad. Sci. U. S. A. 89 (1992) 8721–8725.
[16] M.K. Khan, H. Rahaman, F. Ahmad, Conformation and thermodynamic stability of pre-molten and molten globule states of mammalian cytochromes-c, Metallomics 3 (2011) 327–338.
[17] J.L. Neira, NMR as a tool to identify and characterize protein folding intermediates, Arch. Biochem. Biophys. 531 (2013) 90–99.
[18] R. Santucci, F. Sinibaldi, L. Fiorucci, Protein folding: unfolding and misfolding: role played by intermediate states, Mini. Rev. Med. Chem. 8 (2008) 57–62.
[19] R.L. Baldwin, G.D. Rose, Molten globules: entropy-driven conformational change and protein folding, Curr. Opin. Struct. Biol. 23 (2013) 4–10.
[20] J.M. Khan, S.A. Abdulrehman, F.K. Zaidi, S. Gourinath, R.H. Khan, Hydrophobicity alone can not trigger aggregation in protonated mammalian serum albumins, Phys. Chem. Chem. Phys. 16 (2014) 5150–5161.
[21] J.M. Khan, P. Sharma, K. Arora, N. Kishor, P. Kaila, P. Guptasarma, The Achilles' heel of ultrastable hyperthermophile proteins: submillimolar concentrations of SDS stimulate rapid conformational change, aggregation,and amyloid formation in proteins carrying overall positive charge, Biochemistry 55 (28) (2016) 3920–3936.
[22] S. Lindman, W.F. Xue, O. Szczepankiewicz, M.C. Bauer, H. Nilsson, S. Linse, Salting the charged surface: pH and salt dependence of protein G B1 stability, Biophys. J. 90 (8) (2006) 2911–2921.
[23] J.E. Debreczeni, G. Bunkóczi, B. Girmann, G.M. Sheldrick, In-house phase determination of the lima bean trypsin inhibitor: a low-resolution sulfur-SAD case, Acta Crystallogr. D Biol. Crystallogr. 59 (2003) 393–395.
[24] S. Velankar, P. McNeil, V. Mittard-Runte, A. Suarez, D. Barrell, R. Apweiler, K. Henrick, E-MSD: an integrated data resource for bioinformatics, Nucleic Acids Res. 33 (2005) D262–265.
[25] R. Kumar, P. Tripathi, F.R. de Moraes, I.P. Caruso, M.V. Jagannadham, Identification of folding intermediates of streblin, the most stable serine protease: biophysical analysis, Appl. Biochem. Biotechnol. 172 (2014) 658–671.
[26] D. Matulis, R. Lovrien, 1-Anilino-8-naphthalene sulfonate anion-protein binding depends primarily on ion pair formation, Biophys. J. 74 (1) (1998) 422–429.
[27] P. Hammarström, X. Jiang, S. Deechongkit, J.W. Kelly, Anion shielding of electrostatic repulsions in transthyretin modulates stability and amyloidosis: insight into the chaotrope unfolding dichotomy, Biochemistry 40 (38) (2001) 11453–11459.
[28] F. Rashid, S. Sharma, B. Bano, Comparison of guanidine hydrochloride (GdnHCl) and urea denaturation on inactivation and unfolding of human placental cystatin (HPC), Protein J. 24 (2005) 283–292.
[29] Z.M. Scholtz, D. Barrick, E.J. York, J.M. Stewart, R.L. Baldwin, Urea unfolding of peptide helices as a model for interpreting protein unfolding, Proc. Natl. Acad. Sci. U. S. A. 92 (1995) 185–189.
[30] E. Ahmad, P. Sen, R.H. Khan, Structural stability as a probe for molecular evolution of homologous albumins studied by spectroscopy and bioinformatics, Cell Biochem. Biophys. 61 (2011) 313–325.
[31] R. Srinivasan, E.M. Jones, K. Liu, J. Ghiso, R.E. Marchant, M.G. Zagorski, pH-Dependent amyloid and protofibril formation by the ABri peptide of familial british dementia, J. Mol. Biol. 333 (2003) 1003–1023.
[32] S. Ghosh, S. Dolai, J. De, Amyloid fibril formation by pepsin in neutral pH at room temperature, Soft Matter 9 (2013) 11457.
[33] M.G. Di Carlo, V. Minicozzi, V. Foderà, V. Militello, V. Vetri, S. Morante, M. Leone, Thioflavin T templates amyloid β(1–40) conformation and aggregation pathway, Biophys. Chem. 206 (2015) 1–11.
[34] C. Wu, Z. Wang, H. Lei, Y. Duan, M.T. Bowers, J.E. Shea, The binding of thioflavin T and its neutral analog BTA-1 to protofibrils of the Alzheimer's disease Abeta (16–22) peptide probed by molecular dynamics simulations, J. Mol. Biol. 384 (2008) 718–729.
[35] J. Duboisset, P. Ferrand, W. He, X. Wang, H. Rigneault, S. Brasselet, Thioflavine-T and Congo Red reveal the polymorphism of insulin amyloid fibrils when probed by polarization-resolved fluorescence microscopy, J. Phys. Chem. B 117 (2013) 784–788.
[36] M. Priyadarshini, B. Bano, Conformational changes during amyloid fibril formation of pancreatic thiol proteinase inhibitor: effect of copper and zinc, Mol. Biol. Rep. 39 (2012) 2945–2955.
[37] J.O. Matos, G. Goldblatt, J. Jeon, B. Chen, S.A. Tatulian, Pyroglutamylated amyloid-β peptide reverses cross β-sheets by a prion-like mechanism, J. Phys. Chem. B 118 (2014) 5637–5643.
[38] J.M. Khan, S.A. Abdulrehman, F.K. Zaidi, S. Gourinath, R.H. Khan, Hydrophobicity alone can not trigger aggregation in protonated mammalian serum albumins, Phys. Chem. Chem. Phys. 16 (2014) 5150–5161.
[39] W. Qiang, W.M. Yau, J. Schulte, Fibrillation of β amyloid peptides in the presence of phospholipid bilayers and the consequent membrane disruption, Biochim. Biophys. Acta 2015 (1848) 266–276.
[40] W. Qiang, W.M. Yau, R. Tycko, Structural evolution of Iowa-mutant β-amyloid fibrils from polymorphic to homogeneous states under repeated seeded growth, J. Am. Chem. Soc. 133 (2011) 4018–4029.
[41] N. Norlin, M. Hellberg, A. Filippov, A.A. Sousa, G. Gröbner, R.D. Leapman, N. Almqvist, O.N. Antzutkin, Aggregation and fibril morphology of the Arctic mutation of Alzheimer's Aβ peptide by CD, TEM, STEM and in situ AFM, J. Struct. Biol. 180 (2012) 174–189.
[42] S. Chakraborty, V. Ittah, P. Bai, L. Luo, E. Haas, Z. Peng, Structure and dynamics of the alpha-lactalbumin molten globule: fluorescence studies using proteins containing a single tryptophan residue, Biochemistry 40 (2001) 7228–7238.
[43] N. Singh, R. Kumar, M.V. Jagannadham, A.M. Kayastha, Evidence for a molten globule state in Cicer α-galactosidase induced by pH, temperature, and guanidine hydrochloride, Appl. Biochem. Biotechnol. 169 (2013) 2315–2325.
[44] L. Bian, X. Ji, Distribution, transition and thermodynamic stability of protein conformations in the denaturant-induced unfolding of proteins, PLoS One 9 (2014) e91129.
[45] J.M. Khan, A. Qadeer, E. Ahmad, R. Ashraf, B. Bhushan, S.K. Chaturvedi, G. Rabbani, R.H. Khan, Monomeric banana lectin at acidic pH overrules conformational stability of its native dimeric form, PLoS One 8 (2013) e62428.
[46] R. Kenoth, R.K. Kamlekar, D.K. Simanshu, Y. Gao, L. Malinina, F.G. Prendergast, J.G. Molotkovsky, D.J. Patel, S.Y. Venyaminov, R.E. Brown, Conformational folding and stability of the HET-C2 glycolipid transfer protein fold: does a molten globule-like state regulate activity, Biochemistry 50 (2011) 5163–5171.
[47] R.A. Silva-Lucca, S.S. Andrade, R.S. Ferreira, M.U. Sampaio, M.L. Oliva, Unfolding studies of the cysteine protease baupain, a papain-like enzyme from leaves of Bauhinia forficata: effect of pH, guanidine hydrochloride and temperature, Molecules 19 (2013) 233–246.
[48] O.B. Ptitsyn, Molten globule and protein folding, Adv. Protein Chem. 47 (1995) 83–229.
[49] H. Bora, S. Garg, P. Sen, D. Kumar, P. Kaur, R.H. Khan, Y.D. Sharma, Plasmodium vivax tryptophan-rich antigen PvTRAg33.5 contains alpha helical structure and multidomain architecture, PLoS One 6 (1) (2011) e16294.
[50] M. Golczak, A. Kirilenko, J. Bandorowicz-Pikula, S. Pikula, Conformational states of annexin VI in solution induced by acidic pH, FEBS Lett. 496 (2001) 49–54.
[51] A.P. Bom, M.S. Freitas, F.S. Moreira, D. Ferraz, D. Sanches, A.M. Gomes, A.P. Valente, Y. Cordeiro, J.L. Silva, The p53 core domain is a molten globule at low pH: functional implications of a partially unfolded structure, J. Biol. Chem. 285 (2010) 2857–2866.